

Predictive Modeling of Vegetative Drought Using ML/DL Approach on Temporal Satellite Data

Jyoti S. Shukla

*Dept. of Electrical Engineering
Indian Institute of Technology
Dharwad, India
jyoti.shukla.21@iitdh.ac.in*

Rahul Jashvantbhai Pandya

*Dept. of Electrical Engineering
Indian Institute of Technology
Dharwad, India
rpandya@iitdh.ac.in*

Abstract—The contemporary drought monitoring approaches are bounded by the need for greater visibility toward potentially hazardous scenarios. Hence, a temporal predictive analysis is aimed in this paper, which will be highly advantageous in subsequent planning for catastrophe mitigation and for presaging the vegetative health or probable drought event. Furthermore, the well-established Machine Learning (ML) models, comprising Random Forest and Ridge regressor, in addition to Deep Learning (DL) models, such as Multilayer Perceptron, 1D-CNN, and Pix2Pix Generative Adversarial Networks (P2P), are implemented across several timeframes of 1, 3, 6, 9, and 12 months. Also, the ML/DL models are trained by utilizing the Vegetative Health Index (VHI) values derived from NOAA/AVHRR satellite data from 1981 to 2022, with the Indian state of Karnataka conforming as the research region. In addition to generating temporal forecasts, the P2P model is further executed to perform an annual seasonal analysis that depicts the variations in dryness over time. Subsequently, the prediction performance is assessed through Mean Squared Error (MSE), Mean Absolute Error (MAE), and Coefficient of Determination (R²) scores. The pattern of prediction accuracy annotated demonstrates more accurate forecasts for durations of one month (short term) with the best R² score, MSE and MAE notching up to 0.88, 0.009, and 0.055, respectively; consequently, as hypothesized, escorted by a decline with widening temporal gaps for future projections such as the yearly level (long term) where the R² score, MSE, and MAE reduced up to 0.60, 0.030 and 0.114 respectively. Also, the seasonal analysis delivered valuable insights into the influences of various climatic factors on the dryness level of the landmass, which will act conducive to better future planning and preparation.

Index Terms—Vegetative Drought, Vegetative Health Index, Machine Learning, Deep Learning, Predictive modeling

I. INTRODUCTION

The expanding popularity and deployment of Machine Learning (ML)/ Deep Learning (DL) methods, aspects of the Artificial Intelligence (AI) lineage, has ascended to numerous applications across various industry domains [1]–[3]; from healthcare to the automation industry to Remote Sensing (RS) applications, the grasp of AI/ML-based approaches is strengthening with their excellent performances. Recently, a substantial upsurge in the application of AI/ML models to data generated from RS is registered, which can be explicated to the public availability of good computational resources and satellite datasets. Correspondingly, several relevant inferences may be derived from the RS data, predominantly in the form of indices that function as markers for various entities, comprising vegetation, water availability, and soil moisture content. Vegetative

Health Index (VHI), Normalized Difference Vegetation Index (NDVI), Vegetation Condition Index (VCI), and Temperature Condition Index (TCI) embody a few such indicators essential for assessing vegetative health.

A. Related Work

Drought constitutes one of the most prevalent natural catastrophes that has perdured to ravage human settlements since time immemorial; in this direction, several research activities adopting different statistical methods are conducted as demonstrated in [1], [4], [5]. In comparison to inferential statistics, the integration of ML for forecasting weather and land-cover conditions synthesized better results. As inputs to these models, numerous indices acquired from the satellite and meteorological database are presented, and the outcomes are annotated. Support Vector Regressor, KNN, Extreme Gradient Boosting, Linear Regression (LR), Decision Tree (DT), Random Forest (RF), and several others constitute some of the most extensively adopted ML models for processing and analyzing temporal data [1], [4], [6]–[10]. Furthermore, concatenating these ML models with statistical tools such as the Mann-Kendall test and Sen's slope estimator module, trend analysis, and trend extraction are executed on various indices such as the Standardized Precipitation Index or rainfall data to detect changes [1], [11]–[14]. Also, different assortments of meteorological and satellite-data-derived indices are concorded to observe the influence on vegetative drought prediction [7], [15]–[17].

Moreover, RS applications are being expanded by consolidating the RS data with DL models; several research studies have employed a multitude of widely recognized DL models for temporal modeling in the recent decade, spanning Recurrent Neural Networks, LSTM, ConvLSTM, ARIMA, UNet, Convolutional Neural Networks (CNN), 1D-CNN, Multilayer Perceptron (MLP), among others [16]–[23]. However, implementation results of such a myriad of models for drought prediction and analysis are restricted by the period of the projections; in many research studies, time-series analysis of land cover and vegetative health is conducted [4], [5], [8], [15], [21]–[27] but for the short-term. Therefore, contemplating the present scenario, it is essential to establish a long-term, speculative assessment of the future state of green cover and develop a strong readiness strategy to counteract any impending negative attributes and occurrences.

This paper presents an ML/DL-based approach for temporal predictive modeling of vegetative health and emphasizes the availability of predictions of vegetative health at different timeframes. Correspondingly, the findings are rigorously evaluated and subsequently segregated to achieve the various drought severity levels through the outputs for different temporalities ranging from a one-month prediction to an annual forecast. In pursuit of the stated goal, ML models accounting for Ridge and RF regressor in tandem with DL models, namely MLP, 1D-CNN, and Pix2Pix Generative Adversarial Networks (GANs), abbreviated P2P, are applied in this work on the NOAA/AVHRR-derived VHI dataset for the timeframes: 1, 3, 6, 9, and 12 months on the Karnataka region. To the best of the author's knowledge, incorporating satellite data on different timeframes alongside the aforementioned ML/DL models for vegetative drought prediction is a unique contribution that deems promising to aid in long-term planning and preparation for combating any unfortunate future event. Additionally, the second novel contribution to this study is the extension of the P2P, a DL-based generative model, for the task of temporal predictions on the satellite dataset.

The paper is structured as follows for the remainder: Dataset information and processing are addressed in Section I. The models' methodologies and descriptions are outlined in Section III. Section IV of the study serves as a compilation and discussion of all the models' findings, and Section V concludes the article.

II. DATASET DEVELOPMENT

This research inscribes the NOAA/AVHRR satellite-data derived VHI dataset acquired from the STAR NESDIS open source portal with a weekly frequency for the period 1981 to 2022. The VHI is a widely adopted index for vegetative applications and agricultural monitoring, derived from satellite data, and is effective for estimating the green cover. Moreover, it is a congregation of two other satellite-data-derived indices, TCI, emanated through temperature values, and VCI, developed through NDVI readings.

A. Study Area

The study area designated for this investigation is the Indian state of Karnataka, which spans an area of 191,791 km² and is located in the southwest of the country (Fig. 1). The state is incredibly diverse, with mountainous terrain, coastal plains, surplus hills, and plateaus, with the Nilgiri Hills marking the site of the state on the juncture of the Western and Eastern Ghats. The state may be categorized into four chorographic landforms: the northern plains, the central highlands, the southern plateau, and the coastal Karnataka region. Owing to the land's altitude, geography, and proximity to the sea, Karnataka harbors volatile weather. Also, it hosts the country's second-largest landmass under rainfed agriculture, with roughly 12 million hectares of area, rendering it a significant location for vegetative health analysis and drought prediction.

B. VHI Data Processing

The daily raw spectral values are acquired from the NOAA/AVHRR series of satellites, which transmits infor-

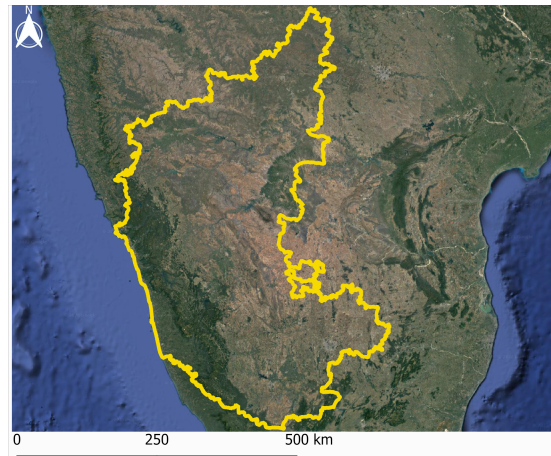


Fig. 1. Study area: The Karnataka state of India.

mation in four-to-six spectral bands and are subsequently preprocessed to develop the VHI index with the assistance of computing NDVI and VCI values. The NOAA STAR open-source portal supplies the weekly global VHI product by merging the 7-days data from which the desired study area is cropped and utilized further. The dataset possessed in this study spans from the 35th week of 1981 to the 25th week of 2022; however, the acquired dataset carries particular missing data points for some weeks, which are populated by executing the mean-refilling technique. As demonstrated in Eq. 1, values for missing weeks are substituted by bearing a mean across all the years with valid values for the same week '*s*' and location '*p*'.

$$\text{VHI value } (p, s) = \frac{\sum(s^{\text{th}} \text{ week for } p^{\text{th}} \text{ location})}{T} \quad (1)$$

In Eq. 1, '*T*' represents the total number of years having the valid VHI values for *p*th location and *s*th week. Consecutively, post-processing, 2123 images from 1981 to 2022 are gathered in aggregate and are further preprocessed to fetch the monthly dataset for temporal modeling.

In this study, the temporal predictions are estimated for monthly timescales of 1, 3, 6, 9, and 12 months, whereby the temporality pertains to the labels assigned for the data samples; for instance, the dataset with a temporality of one month will retain the label for each data point as 1-month time-shifted values. Consequently, the VHI data is scaled between [0,1] along with zero-padding to obtain the structured shape (192,128,1), and henceforth, the dataset development is carried out following the steps annotated in Algorithm 1.

The first segment of Algorithm 1 depicts the transformation of weekly data into monthly data by combining four weeks of information and determining the mean, following which the second half reflects the division of the monthly VHI dataset into several periods. Subsequently, after the conversion from weekly to monthly, the number of data samples is reduced to 531 and is disseminated into different temporal datasets with the labels for the data assigned in accordance with the timeshifts.

After structuring the VHI monthly data into five distinct datasets according to the timeframes, the training and

Algorithm 1: VHI dataset configuration

```

Data: VHI dataset (weekly)
Result: Monthly_data = [ ]
 $l \leftarrow 0$                                  $\triangleright$  Initialize counter ' $l$ '
array  $\leftarrow [0 \dots 0]$ 
for  $x \in (\text{VHI dataset})$  do
    array $+ = x$   $\triangleright$   $x$  is a weekly VHI data sample
     $l+ = 1$ 
    if  $l \% 4 == 0$  and  $l < 53$  then
        array $/ = 4$                                  $\triangleright$  Mean computing
        AppendToMonthly_data  $\leftarrow$  (array)
        if  $l == 52$  then
             $| \quad l \leftarrow 0$                        $\triangleright$  Update counter
        end
    end
end
Data: Monthly_data
Result: Temporal_dataset = [ ],
          Temporal_dataset_label = [ ]
begin
    m  $\leftarrow$  Monthly_data
    t  $\leftarrow$  timescale                          $\triangleright$  Prediction period
    for  $i$  in range ( $\text{len}(m) - t$ ) do
        AppendToTemporal_dataset  $\leftarrow$  m[i]
        AppendToTemporal_dataset_label
         $\leftarrow$  m[i + t]
    end
end

```

testing split is realized with a ratio of 90:10, begetting 45 samples for testing in each dataset. In this study, the months accounted for estimation are cyclical to gain a fair assessment of the extent to which the models produce accurate predictions at various timescales and proffer a seasonal review of vegetative health conditions. This application deems novel concerning the domain of vegetative drought monitoring through AI/ML.

III. METHODOLOGY

The ML/DL paradigm is currently employed in a broad spectrum of domains and has lately been heavily probed for RS applications. This research aims to assess the predictive accuracy of brief (1 month) to protracted (yearly) forecasts and expand the potential avenues of the recognized ML/DL models; the architecture for implementation is demonstrated in Fig. 2.

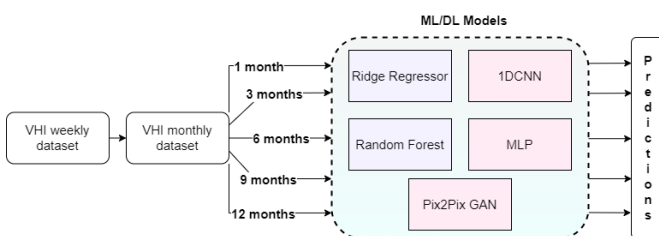


Fig. 2. Temporal predictive modeling of VHI dataset.

A. Ridge Regressor

The Ridge regressor is a modified version of the ML model, LR, that consolidates the linear Ordinary Least Squares (OLS) model and the L_2 regularization term. The Ridge regressor model is preferred when a high proportion of predictor variables are present, for which the LR model struggles to yield satisfactory results. Furthermore, it is favored when the dataset exhibits multicollinearity – in other words, when the independent variables may not be significantly distinctive [28]. In this work, since the data pertains to be periodic and temporal, the drift in values is usually not drastic, and hence LR fails to perform satisfactorily. Contrarily, the Ridge estimator imposes an L_2 penalty on the objective function (L_{RR}) to settle the high variance problem and fits the model more appropriately, as shown in Eq. 2, where y_i is the true value or label for i^{th} sample out of total n samples, x_{ij} represents the j^{th} independent variable for i^{th} input sample, w_j describes the coefficient value for the j^{th} variable, and α designates the magnitude of L_2 penalty to be considered for optimization.

$$L_{RR} = \frac{1}{2n} \sum_{i=1}^n \left(y_i - \sum_j w_j x_{ij} \right)^2 + \frac{\alpha}{2} \sum_j w_j^2 ; \alpha > 0 \quad (2)$$

The first segment of Eq. 2 represents the standard OLS objective function of LR, to which the L_2 regularization term is adhered and imposed on the weights generated by the model to prohibit their values from growing excessively huge or small. Hence, optimizing the objective function through this approach delivers superior outcomes for multicollinear multi-variable input-output instances.

B. Random Forest

The RF regressor projects an addendum to the DT model; it constructs an ensemble learning model utilizing the bagging method and DT model as the baseline algorithm. Moreover, the ensemble learning strategy accrues by averaging the noise in the data and minimizing the variance [24]. RF functions by constructing individual decision trees, wherein the feature importance is computed by imbibing the Gini impurity and then pooling the projections from all trees to derive the final prediction. Subsequently, as indicated in Eq. 3, where \hat{Y} is the final prediction, and X denotes the input matrix, the absolute feature importance is accumulated by accruing up all the t_i tree predictions and dividing it by the aggregate number of these n_{trees} most significant predictors.

$$\hat{Y} = t(X) = \frac{1}{n_{trees}} \sum_{i=1}^{n_{trees}} t_i(X) \quad (3)$$

The RF regressor ranks among the most prominent ML models for handling enormous datasets in regression applications. Moreover, the models supply an averaged response encompassing all the attributes, eliminating overfitting and pursuing feature selection through feature significance computation.

C. Multilayer Perceptron

An MLP is a straightforward DL-based strategy with three or more layers of feedforward neural network architecture; input, hidden, and output layers constitute the fundamental parts of MLP. The information streams through input to the hidden layer (h), passing through an activation function to the output layer, and conclusively, the final value is outputted through another activation function [29].

$$\hat{y}_i = \text{ReLU} \left[\sum_{k=0}^h \left[w_k \sigma \left(\sum_{i=0}^n w_{ki} x_i \right) \right] \right] \quad (4)$$

As demonstrated in Eq. 4, the computation of output \hat{y}_i for x_i , which is i^{th} input sample out of n total samples, through h hidden layers, and w_{ki} symbolizes the weight or coefficient for k^{th} hidden layer and i^{th} input sample. Here, *ReLU* serves as the activation function for the output layer, whereas σ is the *Sigmoid* activation function implemented for the hidden layers; the MLP network developed for this research involves four hidden layers.

D. 1D-CNN

The 1-Dimensional CNN belongs to the class of preferred DL models for temporal estimates, a refinement of the classic CNN primarily intended for processing datasets of 2D images. Analogous to the MLP model, 1D-CNN contains input, hidden, and output layers; nevertheless, the computations between the weights of the filter kernels and the input values conform to the convolutional structure [30]. Moreover, the convolutional layer is often followed by pooling and dropout layers to improve model fitting. As exhibited in Eq. 5, a sequential input vector $X = [X_1, X_2, \dots, X_n]$ of length n is fed to the 1D-CNN model, which further convolves with the filter vector \vec{w} and generates a feature representation F_i .

$$F_i = f(\vec{w} * X_{i:i+d-1}) + b \quad (5)$$

In Eq. 5, f defines the activation function, selected in this work as *ReLU*, for hidden convolutional layers and *Sigmoid* for the final output layer, b is the bias, and $X_{i:i+d-1}$ designates the d -length input window (matches the kernel length) commencing from i^{th} input timestep. Furthermore, a final feature vector representation is constructed by sliding the window over the complete input vector.

E. Pix2Pix GAN

P2P is a cutting-edge model that belongs under the generative subcategory of DL models; GANs are frequently incorporated for generating and expanding datasets. Nevertheless, another subset of GAN models that can develop illustrations relying on a particular entity is conditional GANs (c-GAN); P2P depicts an instance of the c-GAN model, which produces a representation based on another image. The competence of P2P is further expanded in this study by employing it to perform regression tasks and forecasting the forthcoming timestep imagery utilizing the input of the current timestep images. The P2P model comprises two components: a generator, intended to learn from inputs and produce images identical to the label

supplied, and a discriminator, anticipated to distinguish between the image produced by the generator and the original image. Furthermore, the discriminator estimates a probabilistic loss and transmits it to the generator, which then constructs more realistic images contingent on the feedback. An L2 loss function is employed to persecute the generator further and ensure that the resulting image and label are identical [31]. Hence, the adversarial and L2 losses are aggregated to yield the P2P model's overall loss function and induce a dual min-max objective function as revealed in Eq. 6, where the discriminator (D) seeks to maximize the adversarial loss, and the generator (G) aims to reduce it.

$$G^* = \arg \min_G \max_D \{E_{x_i, y_i} [\log D(x_i, y_i)] + E_{x_i, z} [\log(1 - D(x_i, G(x_i, z)))]\} + G_{L2} \quad (6)$$

$$G_{L2} = \lambda E_{x_i, y_i, z} [\|y_i - G(x_i, z)\|_2] \quad (7)$$

In Eq. 6, the first and second elements comprise the log probabilistic losses with relation to the actual and generated images supplied to the discriminator. In contrast, the final segment (G_{L2}) characterizes the L2 norm loss imposed on the generator, shown in Eq. 7, with x_i, y_i accounting for the i^{th} input-label pair of total n samples, respectively, z denotes the instilled random noise, and λ determines the fraction of L2 loss absorbed in the objective function. This study enforces the layered CNN architecture for the discriminator and the UNet encoder-decoder framework as the generator architecture.

F. Implementation and Evaluation Process

According to the timeshifts, the VHI dataset is divided into five datasets: D1 (1 month), D3 (3 months), D6 (6 months), D9 (9 months), and D12 (12 months). Moreover, the timeshifts are quantified in relation to the labels designated to the data; for instance, in D1, a label $y_i = x_i + 1$ for a data sample x_i implies a monthly increment, as demonstrated in Algorithm 1. Subsequently, the datasets are flattened and supplied as inputs for model training; however, the P2P model expects the data in a paired structure, and hence the data-labels pairs are generated and delivered to the P2P model.

$$MSE = \frac{1}{n} \sum_{i=1}^n (y_i - \hat{y}_i)^2 \quad (8)$$

$$MAE = \frac{1}{n} \sum_{i=1}^n |y_i - \hat{y}_i| \quad (9)$$

$$R2 = 1 - \frac{\sum_i (y_i - \hat{y}_i)^2}{\sum_i (y_i - \bar{y})^2} \quad (10)$$

The assessment of the outcomes is conducted based on the evaluation metrics: Mean Squared Error (MSE), which computes the squared error between the true and predicted values and is expected to be minimum for good prediction, Mean Absolute Error (MAE), which computes the difference magnitude between the true and predicted instances and should be minimum, and the Coefficient of Determination (R2) which quantifies the regression fit and

should be towards the higher edge in the range [0,1] for a good fit. Additionally, the derived forecasts are further color-coded to determine the amount of drought severity centered on the VHI values, which range from [0,100]; a value of $VHI < 40$ denotes the presence of drought.

The metric estimations are performed by engrossing the equations displayed in Eq. (8 - 10), where y_i represents the true value or label for the i^{th} input sample of total n samples, \hat{y}_i portrays the predicted value and \bar{y} expresses the mean across all the labels.

IV. RESULTS AND DISCUSSION

This section details the implementation process, the assessment criteria, and the attained outcomes. All the simulations of this research are carried out on a 6 GB NVIDIA RTX (A2000) GPU; furthermore, the obtained results are color-coded to demonstrate the distinct levels of drought severity according to color hues.

A. Prediction Results

The performance metrics, MSE, MAE, and R2, are computed across all the five sub-datasets (D1-D12) and for all the models described formerly. Consequently, the prediction accuracy is represented by the R2 score, whereas loss in predictions is illustrated through MSE and MAE as summarized in Table I for various models throughout the datasets.

TABLE I

EVALUATION METRICS COMPARISON THROUGH ML/DL MODELS FOR DIFFERENT TEMPORALITY

Models/ Datasets	Ridge		RF		MLP		1D-CNN		P2P	
	MSE	MAE	MSE	MAE	MSE	MAE	MSE	MAE	MSE	MAE
D1	0.014	0.066	0.019	0.078	0.019	0.083	0.019	0.078	0.009	0.055
D3	0.017	0.075	0.021	0.083	0.022	0.087	0.024	0.090	0.017	0.075
D6	0.021	0.085	0.022	0.084	0.025	0.093	0.025	0.087	0.021	0.083
D9	0.024	0.088	0.021	0.084	0.028	0.108	0.027	0.091	0.024	0.088
D12	0.023	0.085	0.022	0.085	0.030	0.114	0.028	0.0928	0.026	0.091

Through the curve presented in Fig. 3, the prediction accuracy in terms of the R2 score can be traced. As can be witnessed, the R2 score for D1-D12 varies within the 0.88 – 0.60 range, with the higher values of R2 earned by D1 forecasts for the short temporality and is contrarily least for D12, where an annual prediction is being attempted, and hence temporality is extended.

The trajectory emerges proportionate with high prediction performance for short temporal durations and a deteriorating prediction strength for extended timeframes, as apparent from Table I and Fig. 3, largely for all models. Subsequently, among the models, MLP, 1D-CNN, and P2P convey a persistent reduction in the R2 values, whereas RF demonstrates a saturated performance after the temporality crosses 6 months (D3 onwards). The Ridge regressor persists in the pattern but shoots up for the D12 dataset, implying a gain in predictive ability. Furthermore, the MSE values for the predictions consequently reflect a rise with increasing temporality, with a smaller loss for short-duration forecasts; all models, with the exception of RF, exhibit similar tendencies. Harmonizing to the R2 values, the MAE values similarly indicate an elevation in the error value with increasing temporality, which is congruent with the reduction in R2 values over longer

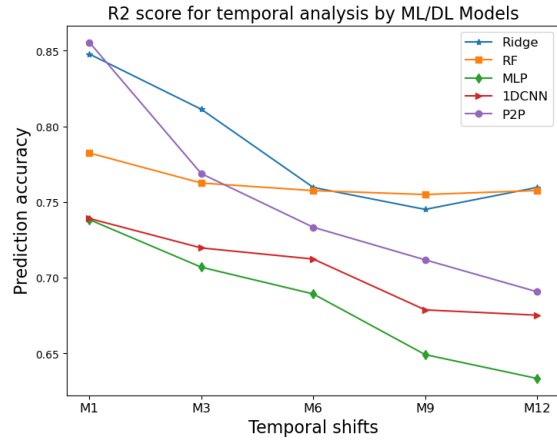


Fig. 3. Prediction accuracy over the datasets for different ML/DL models.

durations. Conclusively, these patterns remain consistent with the predictive trend of producing better forecasts for short-term predictions, whereas projections for long-term instances are impacted due to a decrease in the feature-richness significant for prognosis. Despite the low R2 scores for long-term periods such as D9 or D12, it is feasible to acquire and engage with the supposition for the tentative occurrence of future happenings to construct preventative strategies for any foreseeable drought situation ahead of time.

B. Seasonal Analysis of VHI Variations

The performance measures for the various temporal datasets and models in the preceding section exemplify prediction ability as temporality advances. Moreover, a seasonal study based on the anticipated results of the P2P model is executed in this segment, broadening the generative capacity of the P2P model for protracted forecasts. According to the study, the years 2014 and 2015 have been consecutively affected by a meteorological drought [32]; furthermore, to verify the P2P model's effectiveness for long-term forecasting, the model is accustomed to the 2015 annual data and renders a prediction for 2016. Subsequently, the trained P2P model yields an annual forecast for 2016, a year succeeding the 2015 drought. Additionally, the analysis is expanded to examine the seasonal variations throughout the year and their implications on green cover. Moreover, the yearly forecast demonstrated similar representations for the year 2016 as the ground truth images procuring an excellent R2 score of 0.87, emphasizing the relevance of leveraging the approach for annual prediction in the future. Such yearly or long-term projections are capable of offering a myriad of insights that can assist in planning and preparation. Additionally, color coding is employed to craft a seasonal analysis, highlighting the transitions in land dryness parameters following the drought-hit year.

Precipitation constitutes one of the most critical factors affecting the green cover, even though agricultural drought depends on a multitude of factors. Customarily, the seasonal distribution of rainfall in India is observed through pre-monsoon, or the summer period from March to May, abided by the peak monsoon season, which lasts from June

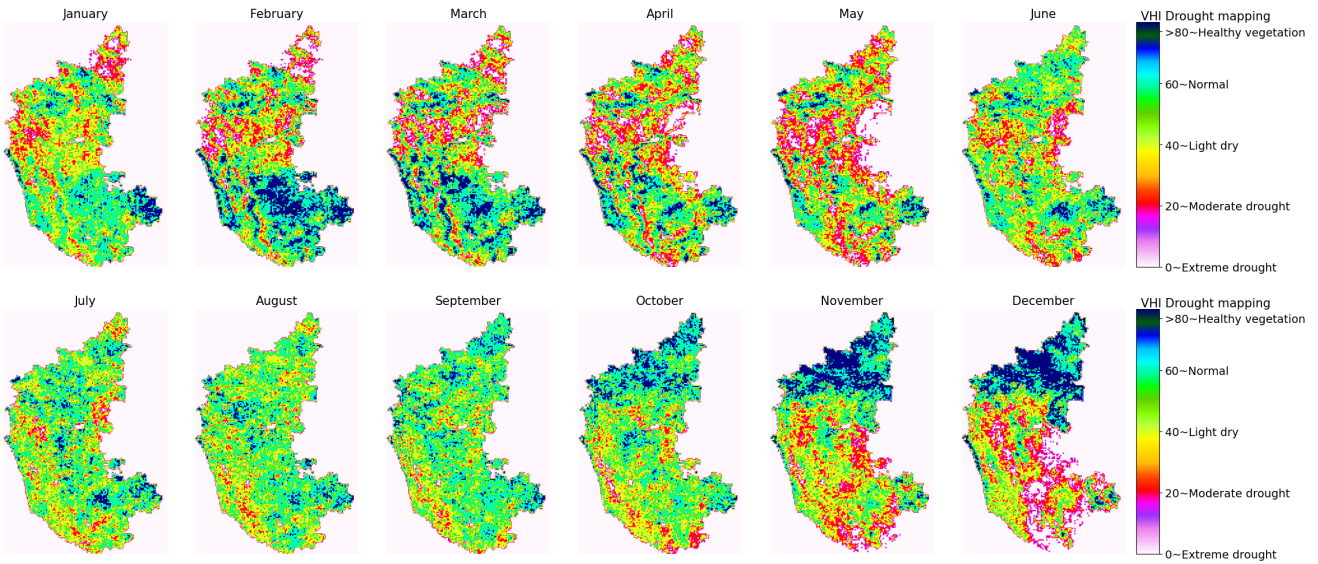


Fig. 4. Annual seasonal analysis through P2P model for the year 2016.

to September, subsequently the post-rainfall months from October to December, and eventual southwest winter-rains in January and February. As apparent from Fig. 4, the green cover diminishes from January to May, encapsulating the pre-monsoon season; nonetheless, the few green components from January to March can be attributed to the winter rains. Eventually, as envisaged throughout the monsoon and post-monsoon months, a noticeable elevation in the greenery is marked, gradually declining towards the end of November and December. Thus to summarize, the monthly scenarios reveal the state being predominantly impacted by post-drought trauma, ranging from light-dry intensity to extreme drought-affected regions. Remarkably, such assortments of predictive analysis may assist organizations in gaining a comprehensive understanding of the future situation and in aiding to ensure the fundamentals for the society, especially for the farmer community, together with food, water, and economic security. Collectively, these investigations benefit in deriving insightful inferences and enhance the preparedness for future catastrophic events.

V. CONCLUSION

This paper presents the predictive modeling of vegetative health status and potential drought scenarios employing ML/DL-based models on temporal satellite data, in addition to an endeavor at the seasonal analysis of the predicted annual forecast. The articulated objective is accomplished by incorporating the NOAA/AVHRR-derived VHI dataset, with Karnataka state as the study area, and then projecting the VHI values at assorted monthly temporalities cumulatively into five dataset configurations: D1 (1 month), D3 (3 months), D6 (6 months), D9 (9 months), and D12 (12 months). Subsequently, Ridge and RF regressor embody the ML models employed that earned significantly good performance metrics with R2 score, MSE, and MAE values in the range of 0.85 – 0.75, 0.014 – 0.023 and 0.066 – 0.085 respectively, for all five temporal datasets produced, although an uneven predictive trend is observed. Alternatively, the DL models subsumed, enclose MLP,

1D-CNN, and P2P, conveying a persistent transition from short-term (1 monthly) to long-term (yearly) forecasts with inferior accuracy for longer temporal durations and higher accuracy for brief periods, rendering them quite reliable in contrast to the ML models with R2 score, MSE, and MAE in the range of 0.88 – 0.60, 0.009 – 0.030 and 0.055 – 0.114 respectively, across all datasets. The P2P model is furthermore operated to elicit a seasonal analysis based on the yearly forecast generated by the model post a drought year and proficiently communicates the greenery alteration of the landmass over the annual period.

The future extent of this paper is to encompass additional meteorological parameters, in addition to VHI, that could alter the green cover and advance the experiments to a broader geographical region. Also, the current study is limited to annual predictions; hence, the temporality of forecasts can be scaled further, and the predictive tendency can be observed by further extrapolating the datasets.

ACKNOWLEDGMENT

This study is being carried out pursuant to the auspices of the ANTRIX Corporation, which assisted in the formation of the Space Data Science Lab at the IIT Dharwad in Karnataka, India. The GPU facility procured through SERB grant number 00047, in conjunction with the DGX GPU rendered by ANTRIX Corporation, is employed partially to conduct the experimental research in this work. Also, the authors acknowledge the guidance and support provided by Dr. Rajshankar V. Bhat, Assistant Professor, IIT Dharwad, towards the conduction of this research.

REFERENCES

- [1] S. Zhong, L. Di, Z. Sun, Z. Xu, and L. Guo, "Investigating the long-term spatial and temporal characteristics of vegetative drought in the contiguous United States," *IEEE J. Sel. Topics Appl. Earth Observ. Remote Sens.*, vol. 12, no. 3, pp. 836–848, Mar. 2019.
- [2] W. Wenxuan, W. Qianshu, H. Chaofan, S. Xizhe, B. Ruiming, and T. T. Toe, "Leaf disease image classification method based on improved convolutional neural network," in *IEEE Int'l Conf. on Industry 4.0, Artificial Intell., and Comm. Tech. (IAICT)*, Sept. 2022, pp. 210–216.

- [3] F. A. Tasa, Istiqomah, M. A. Murti, and I. Alinursafa, "Classification of earthquake vibrations using the ANN (Artificial Neural Network) algorithm," in *IEEE Int'l Conf. on Industry 4.0, Artificial Intell., and Comm. Tech. (IAICT)*, Sept. 2022, pp. 102–107.
- [4] A. Shahabfar, A. Ghulam, and C. Conrad, "Understanding hydrological repartitioning and shifts in drought regimes in central and south-west Asia using MODIS derived perpendicular drought index and TRMM data," *IEEE J. Sel. Topics Appl. Earth Observ. Remote Sens.*, vol. 7, no. 3, pp. 983–993, Oct. 2014.
- [5] S. Liu, J. Tian, S. Wang, D. Wang, T. Chi, and Y. Zhang, "Crop drought area extraction based on remote sensing time series spatial-temporal fusion vegetation index," in *IEEE Int'l Geosci. and Rem. Sens. Symp. (IGARSS)*, Nov. 2019, pp. 6271–6274.
- [6] S. Y. J. Prasetyo, K. D. Hartomo, M. C. Paseleng, D. W. Candra, and B. H. Simanjuntak, "The machine learning to detect drought risk in central Java using Landsat 8 OLI remote sensing images," in *5th Int'l Conf. on Science and Tech. (ICST)*, vol. 1, Jul. 2019, pp. 1–6.
- [7] Z. Zhang, W. Xu, Z. Shi, and Q. Qin, "Establishment of a comprehensive drought monitoring index based on multisource remote sensing data and agricultural drought monitoring," *IEEE J. Sel. Topics Appl. Earth Observ. Remote Sens.*, vol. 14, pp. 2113–2126, Jan. 2021.
- [8] G. Berhan, S. Hill, T. Tadesse, and S. Atnafu, "Drought prediction system for improved climate change mitigation," *IEEE Trans. on Geosci. and Remote Sens.*, vol. 52, no. 7, pp. 4032–4037, Oct. 2014.
- [9] S. Perera, W. Li, E. Linstead, and H. El-Askary, "Forecasting vegetation health in the MENA region by predicting vegetation indicators with machine learning models," in *IEEE Int'l Geosci. and Rem. Sens. Symp. (IGARSS)*, Oct. 2020, pp. 4642–4645.
- [10] E. Sreehari and S. Srivastava, "Prediction of climate variable using multiple linear regression," in *4th Int'l Conf. on Comp. Comm. and Automat. (ICCCA)*, Dec. 2018, pp. 1–4.
- [11] Z. Xu, L. Cao, S. Zhong, G. Liu, Y. Yang, S. Zhu, X. Luo, and L. Di, "Trends in global vegetative drought from long-term satellite remote sensing data," *IEEE J. Sel. Topics Appl. Earth Observ. Remote Sens.*, vol. 13, pp. 815–826, Feb. 2020.
- [12] Z. Zhang, W. Xu, Q. Qin, and Y. Chen, "Monitoring and assessment of agricultural drought based on solar-induced chlorophyll fluorescence during growing season in north China plain," *IEEE J. Sel. Topics Appl. Earth Observ. Remote Sens.*, vol. 14, pp. 775–790, Oct. 2021.
- [13] J. Lu, L. Jia, C. Zheng, J. Zhou, M. V. Hoek, and K. Wang, "Characteristics and trends of meteorological drought over China from remote sensing precipitation datasets," in *IEEE Int'l Geosci. and Rem. Sens. Symp. (IGARSS)*, Nov. 2016, pp. 7581–7584.
- [14] F. Muthoni, "Spatial-temporal trends of rainfall, maximum and minimum temperatures over west Africa," *IEEE J. Sel. Topics Appl. Earth Observ. Remote Sens.*, vol. 13, pp. 2960–2973, May 2020.
- [15] D. Yang, S. Zhong, X. Mei, F. Niu, and W. Zhu, "Correlation analysis of vegetation drought and influencing factors and a preliminary prediction model based on convolutional LSTM," in *10th Int'l Conf. on Agro-Geoinfo. (Agro-Geoinformatics)*, Aug. 2022, pp. 1–6.
- [16] M. Jalili, J. Gharibshah, S. M. Ghavami, M. Beheshtifar, and R. Farshi, "Nationwide prediction of drought conditions in Iran based on remote sensing data," *IEEE Trans. on Comp.*, vol. 63, no. 1, pp. 90–101, May 2014.
- [17] H. Balti, A. B. Abbes, N. Mellouli, Y. Sang, I. R. Farah, M. Lamolle, and Y. Zhu, "Big data based architecture for drought forecasting using LSTM, ARIMA, and Prophet: Case study of the Jiangsu province, China," in *2021 Int'l Congress of Advanced Tech. and Engineering (ICOTEN)*, Jul. 2021, pp. 1–8.
- [18] C. Liu, H. Li, A. Su, S. Chen, and W. Li, "Identification and grading of maize drought on RGB images of UAV based on improved U-Net," *IEEE Geoscience and Remote Sens. Letters*, vol. 18, no. 2, pp. 198–202, 2021.
- [19] D. Hong and K. A. Hong, "Drought forecasting using MLP neural networks," in *8th Int'l Conf. on u- and e-Service, Science and Tech. (UNESST)*, Nov. 2015, pp. 62–65.
- [20] K. S. Dayal, R. C. Deo, and A. A. Apan, "Application of hybrid artificial neural network algorithm for the prediction of standardized precipitation index," in *IEEE Region 10 Conf. (TENCON)*, Nov. 2016, pp. 2962–2966.
- [21] W. Tian, J. Wu, H. Cui, and T. Hu, "Drought prediction based on feature-based transfer learning and time series imaging," *IEEE Access*, vol. 9, pp. 101454–101468, Jul. 2021.
- [22] S. Zhong, Z. Xu, and L. Cao, "Evaluating performance of prediction of vegetative drought using classic and recent sequence-based models," in *9th Int'l Conf. on Agro-Geoinfo. (Agro-Geoinformatics)*, Sept. 2021, pp. 1–6.
- [23] U. Ashwini, K. Kalaivani, K. Ulagapriya, and A. Saritha, "Time series analysis based Tamilnadu monsoon rainfall prediction using seasonal ARIMA," in *6th Int'l Conf. on Inventive Comp. Tech. (ICICT)*, Feb. 2021, pp. 1293–1297.
- [24] S. Shamshirband, S. Hashemi, H. Salimi, S. Samadianfar, E. Asadi, S. Shadkani, K. Kargar, A. Mosavi, N. Nabipour, and K.-W. Chau, "Predicting standardized streamflow index for hydrological drought using machine learning models," *Engineering Apps. of Comp. Fluid Mech.*, vol. 14, no. 1, pp. 339–350, Jan. 2020.
- [25] J. Lu, L. Jia, J. Zhou, C. Zheng, and G. Hu, "Adaptability of six global drought indices over China," in *IEEE Int'l Geosci. and Rem. Sens. Symp. (IGARSS)*, Nov. 2019, pp. 9922–9925.
- [26] P. Zhang, L. Zhang, H. Leung, and J. Wang, "A deep-learning based precipitation forecasting approach using multiple environmental factors," in *IEEE Int'l Congress on Big Data (BigData Congress)*, Sept. 2017, pp. 193–200.
- [27] Y. Dhyani and R. J. Pandya, "Deep learning oriented satellite remote sensing for drought and prediction in agriculture," in *IEEE 18th India Council Int'l Conf. (INDICON)*, Dec. 2021, pp. 1–5.
- [28] D. Chumachenko, K. Bazilevych, I. Meniailov, S. Yakovlev, and T. Chumachenko, "Simulation of COVID-19 dynamics using ridge regression," in *IEEE 4th Int'l Conf. on Advanc. Info. and Comm. Tech. (AICT)*, Dec. 2021, pp. 163–166.
- [29] N. A. Agana and A. Homaifar, "A deep learning based approach for long-term drought prediction," in *SoutheastCon*, May 2017, pp. 1–8.
- [30] F. Husari and J. Seshadrinath, "Early stator fault detection and condition identification in induction motor using novel deep network," *IEEE Trans. on Artificial Intell.*, vol. 3, no. 5, pp. 809–818, Dec. 2022.
- [31] P. Isola, J. Y. Zhu, T. Zhou, and A. A. Efros, "Image-to-Image translation with Conditional Adversarial Networks," in *IEEE Conf. on Comp. Vis. and Patt. Recog. (CVPR)*, Nov. 2017, pp. 5967–5976.
- [32] G. o. I. Ministry of Agriculture & Farmers' Welfare, "Drought management," Accessed Apr. 2023.